

Design and Flight Testing of the Ducted-fan UAV Flight Array System

Taegyun Kim¹, Hoiho Jeong¹, Seongyoung Kim¹, Inrae Kim¹, Seungkeun Kim^{1*}, Jinyoung Suk¹ and Hyo-Sang Shin²

^{1*}Department of Aerospace Engineering, Chungnam National University, 34134, Daejeon, Republic of Korea.

²School of Aerospace, Transport and Manufacturing, Cranfield University, MK43 0AL, Cranfield, UK.

*Corresponding author(s). E-mail(s): skim78@cnu.ac.kr;
Contributing authors: ktg92@o.cnu.ac.kr; jeonghoiho@cnu.ac.kr;
ks8600@hanmail.net; irkim91@o.cnu.ac.kr; jsuk@cnu.ac.kr;
h.shin@cranfield.ac.uk;

Abstract

This study proposes a ducted-fan flight array (DFA) system that can change the array based on the mission environment and validate the feasibility through ground and flight tests. This DFA can carry out normal formation flight as separated UAV members and can also cooperate as a single entity by physical connection. The ducted-fan unmanned aerial vehicle (UAV) is manufactured in-house and equipped with a connected surface and an assembly device on the side to perform connection and separation tasks. Moreover, the control system was designed using an open-source autopilot environment, and the communication environment for multi-UAV flight was constructed using the Robot Operating System (ROS). Then, ground and preliminary experimental tests verified the feasibility and performance of the DFA system for connected and separated flight.

Keywords: Ducted-fan flight array system, Unmanned aerial vehicle, Formation flight, Flight test

1 Introduction

Unmanned aerial vehicles (UAVs) are employed in various real-life applications, such as surveillance and reconnaissance. Because of their ability to reduce the risk to humans and provide cost-effective options in several conditions where they cannot use the operating system. Specifically, vertical take-off and landing (VTOL) UAVs are aircraft that take off, land, and hover the same as rotary-wing aircraft, which are less affected by the take-off/landing places[1]. However, it has a disadvantage in that it is not as efficient as a fixed-wing aircraft.

For this reason, a ducted fan UAV platform was proposed to improve these shortcomings, and a duct could improve thrust efficiency. In addition, since the duct is wrapped around the rotor, it has the advantage of being safe during operation, so its usability is increasing. However, despite this increase in efficiency, VTOL UAVs have many factors to overcome to cover large areas. In addition, adding a duct has a disadvantage in that it is weak to disturbance and difficult to operate in adverse conditions [2].

As an alternative to solve these problems, a multi-flight system in which several aircraft fly simultaneously is introduced. The multi-flight system can simultaneously perform missions with the development of communication technologies [3], [4], and can acquire more data, occupy broader areas, and lift heavier objects especially in surveillance and scouting missions than operating a single UAV [5]. Additionally, it is being researched to be used in various fields by making it a connected UAV platform to withstand disturbances robustly.

1.1 Related work

In order to improve practical performance, the ducted-fan UAV is driving evident interest in academics. Compared with the open-rotor UAV, it is known that the ducted-fan UAV has many inherent advantages, e.g., thrust efficiency and safety. These advantages enable ducted-fan UAVs to achieve various applications in unknown, dangerous conditions and difficult for traditional open-rotor UAVs. Deng et al. [6] experimentally validated the ducted-fan UAV's force and pressure model using particle image velocimetry (PIV) measurements on hover and forward flight conditions. In addition, the experiment analyzed aerodynamic factors and their effect on the duct lip. Cheng and Pei [7] conducted the control design on the transition of the ducted-fan UAV from hover to forward flight.

Recently, various studies have been conducted to extend ducted-fan UAV's advantages to connected vehicles for various flight missions. ETH Zürich in Switzerland conducted a distributed flight array study in which several modular VTOL UAVs were combined into a specific shape on the ground and then flew [8]. In addition, three-combined-shaped aerial vehicles were manufactured and tested with ducted-fan UAVs, each with one control flap [9]. In a similar way, the International Islamic University of Malaysia conducted a study in which two triangular UAVs flew together as connected [10]. Fan et al. [11]

proposed a platform combining two ducted-fan UAVs and performed simulation and flight tests to analyze flight performance. After that, the manipulator was mounted under the connected vehicles for the flight test to verify the robustness against faulty situations [12]. However, these related studies have the limitation that the UAVs can fly only in a combined state and cannot be separated or operated individually.

1.2 Main contribution

This study proposes a novel system that can be operated differently depending on the mission and situation beyond the simple multi-flight operation. A ducted-fan flight array (DFA) is composed of multiple ducted-fan UAVs that can fly individually and perform cooperating and distributed flights based on their flight missions. Moreover, this system operates as a single unit but performs tasks that cannot be conventionally performed by a single unit, including operations in a disturbed environment, through connected action and separation. The main contributions of this study are as follows:

- The novel platform system enables existing UAVs to perform tasks that they fail to perform initially, such as cooperative missions and heavy lifts.
- It can be connected and separated depending on the mission and UAV state situation, enabling single or multiple UAV operation and flexible response.
- To validate the proposed DFA concept, ducted-fan UAVs and connecting devices are designed and manufactured in-house.

After performing the validation through numerical simulations with dynamic modeling, subsequent preliminary flight tests were performed for single-unit flight, formation flight as separated entities, and connected flight as a single DFA entity with in-flight separation. These successive experimental results show that the DFA can be effectively used for solo and group flights. In particular, the separation experiment proves that separating a DFA in the air is possible.

This paper is organized as follows: Section 2 discusses the DFA system and the development of the ducted-fan UAV. In addition, Section 3 describes the results of the flight tests for essential flight missions in the operation of the DFA system that performs the formation, connection, and separation flights. The study is concluded in Section 4.

2 Ducted-fan UAV Flight Array

2.1 Ducted-fan UAV Flight Array system

The DFA system consists of multiple ducted-fan UAVs that can individually fly, perform, cooperate and distribute flights based on their given flight missions [13], [14], as shown in Figure 1. Moreover, this system operates in various applications and tasks, including reconnaissance, surveillance, and communication relay, that a single-unit UAV operation cannot do. This section introduces

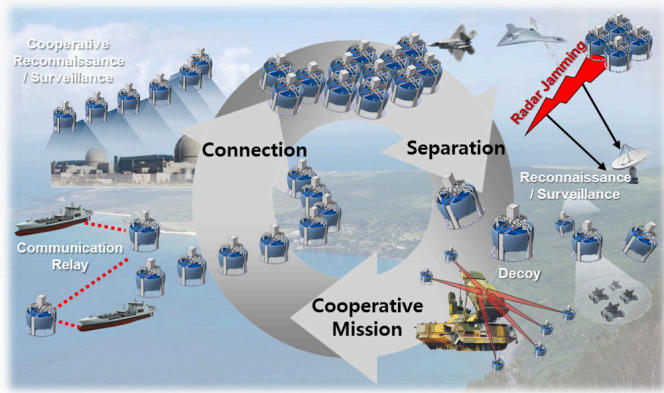


Fig. 1 Operational concept of the DFA system

the design and fabrication of a ducted-fan UAV, which considers the DFA mission [15]. The design of the ducted-fan UAV consists of an avionics system and a motor that generates thrust. This stator cancels out the anti-torque generated by the main rotor, a control system that controls the thrust direction of the UAV, and four assembly devices that are installed in the duct section at 90-degree intervals. Figure 2 shows a design of the ducted-fan UAV.

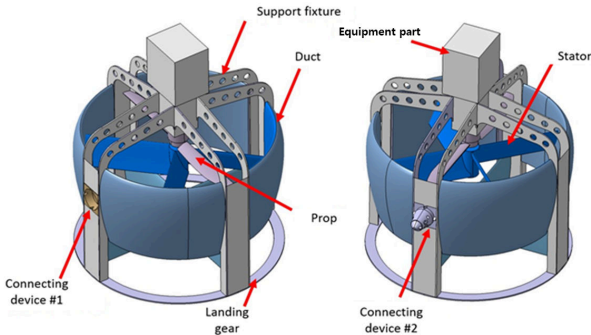


Fig. 2 Design of the ducted-fan UAV

The avionics system is composed of a flight control computer (FCC) and a mission computer for the robot operating system (ROS) communication operations. The motor uses a BLDC motor and is accompanied by a stator at the center of the UAV.

2.2 Dynamic modeling

2.2.1 Ducted-fan UAV model

We analyzed the design and aerodynamics of a ducted-fan UAV using the ducted-fan design calculation (DFDC) software provided by MIT [16]. This

software can calculate the ducted-fan UAV's required thrust and stator geometry based on its two-dimensional shape and the operating environment. We applied a Clark-Y airfoil with a flat bottom of the airfoil for the duct shape to reduce the difference with the connecting surface Table 1 summarizes its numerical parameters. In Table 1, $C_{D,x}$ and $C_{D,y}$ represent the drag coeffi-

Table 1 Parameters of the single ducted-fan UAV

Component	Parameter	Value	Unit
Duct (Airfoil: Clark-Y)	$C_{D,x} = C_{D,y}$	0.5	
	S_{duct}	0.06324	m^2
	c_{duct}	0.17	m
	l_{duct}	0.3	m
Control flaps (Airfoil: NACA0012)	S_{flap}	0.014	m^2
	c_{flap}	0.1	m
	l_{flap}	0.11	m

icients on the body-fixed frame. S_{duct} and S_{flap} denote the frontal area of the duct and flap, respectively. c_{duct} and c_{flap} represent the chords of the duct and flap. l_{duct} and l_{flap} are the distances between the center of gravity, the duct's quarter chord, and the quarter chord of the flap, respectively.

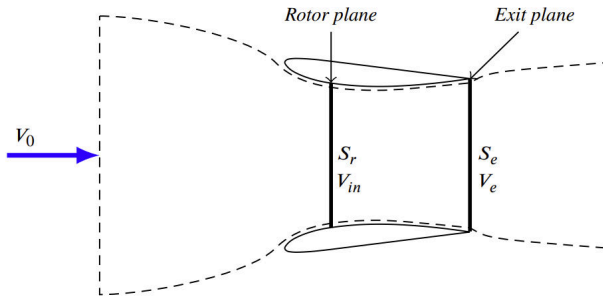


Fig. 3 Control variable of the duct

In order to calculate induced velocities through the rotor, the thrust model generated by the rotor with a ducted-fan is applied as [17]:

$$T = \dot{m}V_e. \quad (1)$$

Assuming incompressible flow, the mass flow rate \dot{m} as shown in Figure 3 is derived from the law of conservation of mass as

$$\dot{m} = \rho S_r V_{in} = \rho S_e V_e \quad (2)$$

where V_{in} represents the induced velocity generated by the rotor. Then, the induced velocity at the end of the duct V_e is defined as follows:

$$V_e = \frac{V_{in}}{\sigma_d} \quad (3)$$

where σ_d is the expansion ratio of the rotor with the duct, which is calculated as the ratio of the duct exit area S_e to the rotor area S_r :

$$\sigma_d = \frac{S_e}{S_r} \quad (4)$$

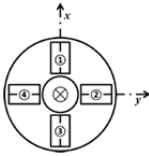
Equation (1) can be rewritten as follows:

$$T = \dot{m}V_e = \rho S_e V_e^2 = \rho S_r \frac{V_{in}^2}{\sigma_d} \quad (5)$$

From Equation (5), the inducted velocity V_{in} can be defined as follows:

$$V_{in} = \sqrt{\frac{T\sigma_d}{\rho S_r}} \quad (6)$$

There are four control surfaces along the x- and y-axes of the body-fixed frame as denoted in Figure 4.



Sense	Control Surface	Effect
δ_{ail}	1, 3	M_x
δ_{ele}	2, 4	M_y
δ_{rud}	1, 2, 3, 4	M_z

Fig. 4 Control surface effects

where M_x , M_y , and M_z are moment components along the body axes. The control surfaces are modeled as follows:

$$F_{sf} = \begin{bmatrix} \text{sgn}(V_e - w)q_e C_{L,sf} \delta_{ele} S_{ele} \\ -\text{sgn}(V_e - w)q_e C_{L,sf} \delta_{ail} S_{ail} \\ 0 \end{bmatrix} \quad (7)$$

$$M_{sf} = \begin{bmatrix} -F_{sf,y} l_{ail} \\ F_{sf,x} l_{ele} \\ \text{sgn}(V_e - w)q_e C_{L,sf} \delta_{rud} l_{rud} \end{bmatrix}$$

where F_{sf} is the external force by the control surfaces, and M_{sf} is the moment by the control surfaces. $C_{L,sf}$ is the lift coefficient of the control surface. δ_{ail} , δ_{ele} , and δ_{rud} represent the deflection angles of the aileron, elevator, and rudder, respectively. q_e is the dynamic pressure at the duct exit, given by

$$q_e = \frac{1}{2}\rho(V_e - w)^2. \quad (8)$$

2.2.2 Stator model

Controlling the ducted-fan UAV requires offsetting the anti-torque generated by the rotor, which is mounted at the center of the UAV [18]. The torque offset force generated from the stator was calculated using DFDC. The thrust T and torque τ equations are shown in Equation. (9).

$$\begin{aligned} T &= T_{rotor} + T_{stator} = b_{thr,1}RPM + b_{thr,2}RPM^2, \\ \tau &= \tau_{rotor} + \tau_{stator} = b_{tor,1}RPM + b_{tor,2}RPM^2, \end{aligned} \quad (9)$$

The results for the anti-torque offset values calculated using DFDC in which stator was fixed at 10° are listed in Table 2.

Table 2 Anti-torque offset value depending on the stator's degree

Degree	9°	10°	11°
τ rotor	0.4478	0.4478	0.4478
τ stator	-0.4397	-0.4465	-0.4532
Sum	0.0081	0.0013	-0.0054

where $b_{thr,1}$ and $b_{thr,2}$ are the thrust coefficients of the rotor and stator, respectively, and $b_{tor,1}$ and $b_{tor,2}$ are the torque coefficients of the rotor and stator, respectively. The stator's airfoil used in the study was the s4083-il, which has a high lift coefficient even at low Reynolds numbers.

2.2.3 Dynamics of the Ducted-fan UAV

The dynamics for the ducted-fan UAV is given as [19]

$$\begin{aligned} \dot{\underline{x}}(t) &= f(\underline{x}(t), \underline{u}(t)), \\ \underline{x} &= [u \ v \ w \ p \ q \ r \ \phi \ \theta \ \psi]^T, \\ \underline{u} &= [\delta_{th} \ \delta_{ail} \ \delta_{ele} \ \delta_{rud}]^T, \end{aligned} \quad (10)$$

where $[u \ v \ w]$ and $[p \ q \ r]$ are the velocity and angular rate components in the x,y, and z axes of the coordinate system of the ducted-fan UAV, respectively. In addition, $[\phi \ \theta \ \psi]$ are the Euler angles of the ducted-fan UAV, and \underline{u} is the control input vector in which each variable consists of a throttle, aileron,

elevator, and rudder control inputs. Moreover, the ducted-fan UAV has symmetrical features in the x and y axes [20],[21]. Therefore, the cross-product of the moment of inertia of the ducted-fan UAV is negligible:

$$J_{xy} = J_{xz} = J_{yz} = 0 \quad (11)$$

The equations of motion of the six degrees of freedom are derived using the force and moment acting on the ducted-fan UAV, i.e.:

$$\begin{aligned} \dot{u} &= vr - wq + F_x/m, \\ \dot{v} &= wp - ur + F_y/m, \\ \dot{w} &= uq - vp + F_z/m, \\ \dot{p} &= \{qr(J_{yy} - J_{zz}) + M_x\}/J_{xx}, \\ \dot{q} &= \{pr(J_{zz} - J_{xx}) + M_y\}/J_{yy}, \\ \dot{r} &= \{pq(J_{xx} - J_{yy}) + M_z\}/J_{zz}, \end{aligned} \quad (12)$$

where F_x , F_y , and F_z are force components in the x,y, and z axes. J_{xx} , J_{yy} , and J_{zz} are principal moments of inertia on each axis.

2.2.4 Dynamics of the Connected Ducted-fan UAV

The DFA can be a reconfigurable system based on multiple ducted-fan UAVs. The numerical model of the DFA considers the ducted-fan UAV dynamics, geometric, and interacting effects. Figure 5 shows a new coordinate system of the DFA when three ducted-fan UAVs are tightly connected.

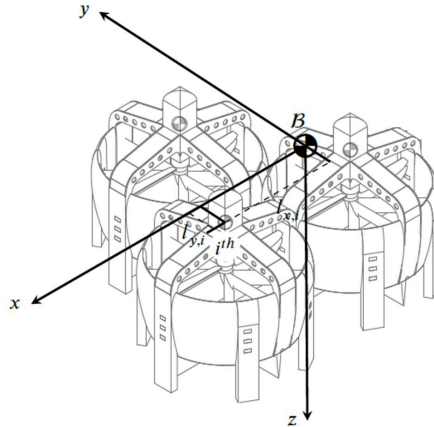


Fig. 5 A conceptual diagram of the connected ducted-fan UAVs as a DFA

For the DFA's connected flight, the forces and moments are given as [23]

$$F = \begin{bmatrix} F_x \\ F_y \\ F_z \end{bmatrix} = \begin{bmatrix} \sum_{i=1}^N F_{x_i} \\ \sum_{i=1}^N F_{y_i} \\ \sum_{i=1}^N F_{z_i} \end{bmatrix} \quad (13)$$

$$M = \begin{bmatrix} M_x \\ M_y \\ M_z \end{bmatrix} = \begin{bmatrix} \sum_{i=1}^N (M_{x_i} - l_{z_i} F_{y_i} + l_{y_i} F_{z_i}) \\ \sum_{i=1}^N (M_{y_i} - l_{x_i} F_{z_i} + l_{z_i} F_{x_i}) \\ \sum_{i=1}^N (M_{z_i} - l_{y_i} F_{x_i} + l_{x_i} F_{y_i}) \end{bmatrix} \quad (14)$$

where l_{x_i} , l_{y_i} , and l_{z_i} indicate the distances between the center of gravity of the DFA and i th ducted-fan UAV, respectively. In this paper, it is assumed that ducted-fan UAVs are connected in the same XY plane. Accordingly, l_{z_i} can be neglected.

2.3 Baseline controller

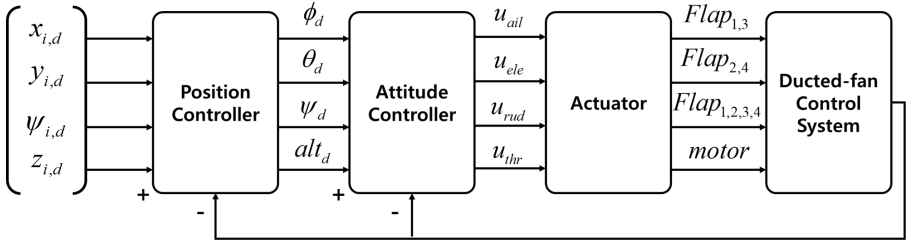


Fig. 6 Diagram of the control system of the ducted-fan UAV

The baseline controller of the ducted-fan UAV is based on the PID controller, which is designed in an angular position and has a rate-cascaded PID inner-outer loop structure provided by Arducopter. Figure 6 shows a flow diagram of the control system of the ducted-fan UAV. The inner loop rate commands are as follows:

$$\begin{aligned} e_p &= K_\phi(\phi_d - \phi) - p, \\ e_q &= K_\theta(\theta_d - \theta) - q, \\ e_r &= K_\psi(\psi_d - \psi) - r, \end{aligned} \quad (15)$$

where ϕ_d , θ_d , and ψ_d are desired attitude commands, and e_p , e_q , and e_r are the inner loop rate errors. Moreover, K_ϕ , K_θ and K_ψ are the proportional gains for the Euler angle error of the outer loop. The virtual control inputs that act

as the aileron, elevator, and rudder can be calculated as:

$$\begin{aligned} u_{ail} &= K_p^p \cdot e_p + K_i^p \int e_p d\tau + K_d^p \frac{de_p}{d\tau}, \\ u_{ele} &= K_p^q \cdot e_q + K_i^q \int e_q d\tau + K_d^q \frac{de_q}{d\tau}, \\ u_{rud} &= K_p^r \cdot e_r + K_i^r \int e_r d\tau + K_d^r \frac{de_r}{d\tau}, \end{aligned} \quad (16)$$

where $K_{p,i,d}^p$, $K_{p,i,d}^q$, and $K_{p,i,d}^r$ denotes the proportional, integral, and derivative gains of the body angular rate (p,q,r) controller. The position controller of the ducted-fan UAV is designed as a P controller. The position error in the inertial frame can be transformed into the body frame position error depending on the current heading angle (ψ) as follows:

$$\begin{aligned} e_{x_body} &= e_{x_in} \cdot \cos \psi + e_{y_in} \cdot \sin \psi \\ e_{y_body} &= e_{y_in} \cdot \cos \psi - e_{x_in} \cdot \sin \psi \end{aligned} \quad (17)$$

where (e_{x_body}, e_{y_body}) and (e_{x_in}, e_{y_in}) are the position errors in the body and inertial coordinate systems, respectively.

2.4 Formation flight algorithm

The ducted-fan UAV of the DFA system moves while maintaining a constant shape for a mission. Thus, in this section, we discuss the computation of the formation method to drive the ducted-fan UAV to the desired formation using a leader-following method, which is illustrated in Figure 7.

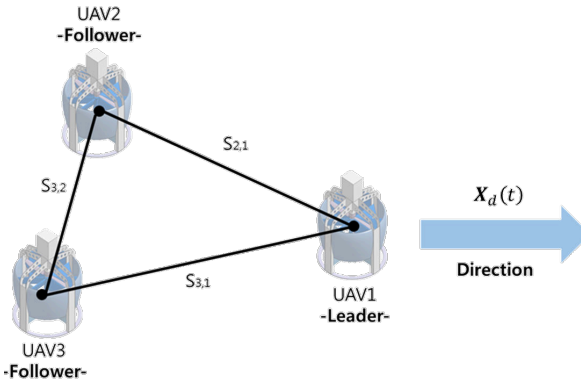


Fig. 7 Leader-follower formation method

The leader-follower formation flight calculates the relative coordinates of the follower UAV based on the position of the leader UAV and maintains the flight through it [24], [25]. Equation (18) defines the desired command of each UAV.

$$X_d(t) = \begin{bmatrix} x_d(t) \\ y_d(t) \\ z_d(t) \\ \psi_d(t) \end{bmatrix} \quad (18)$$

where $x_d(t)$, $y_d(t)$, $z_d(t)$, and $\psi_d(t)$ are the three-dimensional (3D) position desired command value of x , y , z , and ψ , respectively.

The shape of a ducted-fan UAV formation can be calculated by specifying a set of relative position vectors and relative heading values. The vector equation shown in Eq.(19) for the leader-follower formation method is expressed as [26]:

$$S_{i,j} = X_j - X_i = \begin{bmatrix} x_j - x_i \\ y_j - y_i \\ z_j - z_i \\ \psi_j - \psi_i \end{bmatrix} \quad (19)$$

where shape vector $S_{i,j}$ includes the 3D position vector and the yaw angle of the ducted-fan UAV, which uses a 4 x 1 shape vector. The leader-follower formation shape vectors satisfy the following properties:

$$\begin{aligned} S_{i,k} &= S_{i,j} + S_{j,k} \\ S_{i,i} &= [0 \ 0 \ 0]^T \\ S_{i,j} &= -S_{j,i} \end{aligned} \quad (20)$$

2.5 Simulation result

2.5.1 Formation flight simulation

This study numerically validates the formation flight algorithm using the ducted-fan UAV model. We performed a waypoint navigation flight simulation along a set of square paths with a length of 20 m to verify the performance of the leader-follower method. The shape vectors between the leader UAV and follower UAVs are given by Eqs.(21) - (22).

$$S_{F_1,L} = X_L - X_{F_1} = \begin{bmatrix} x_L - x_{F_1} \\ y_L - y_{F_1} \\ z_L - z_{F_1} \end{bmatrix} = \begin{bmatrix} 10 \text{ m} \\ 10 \text{ m} \\ 10 \text{ m} \end{bmatrix} \quad (21)$$

$$S_{F_2,L} = X_L - X_{F_2} = \begin{bmatrix} x_L - x_{F_2} \\ y_L - y_{F_2} \\ z_L - z_{F_2} \end{bmatrix} = \begin{bmatrix} -10 \text{ m} \\ -10 \text{ m} \\ -10 \text{ m} \end{bmatrix} \quad (22)$$

Figure 8 shows the position history of the formation flight in which the red line represents the path of the leader UAV, the black line represents the path of the follower UAV 1, the blue line represents the path of follower UAV 2, and the dotted line represents the command value for each UAV. The simulation results display that the three ducted-fan UAVs perform waypoint flights while maintaining a constant formation based on the commanded shape.

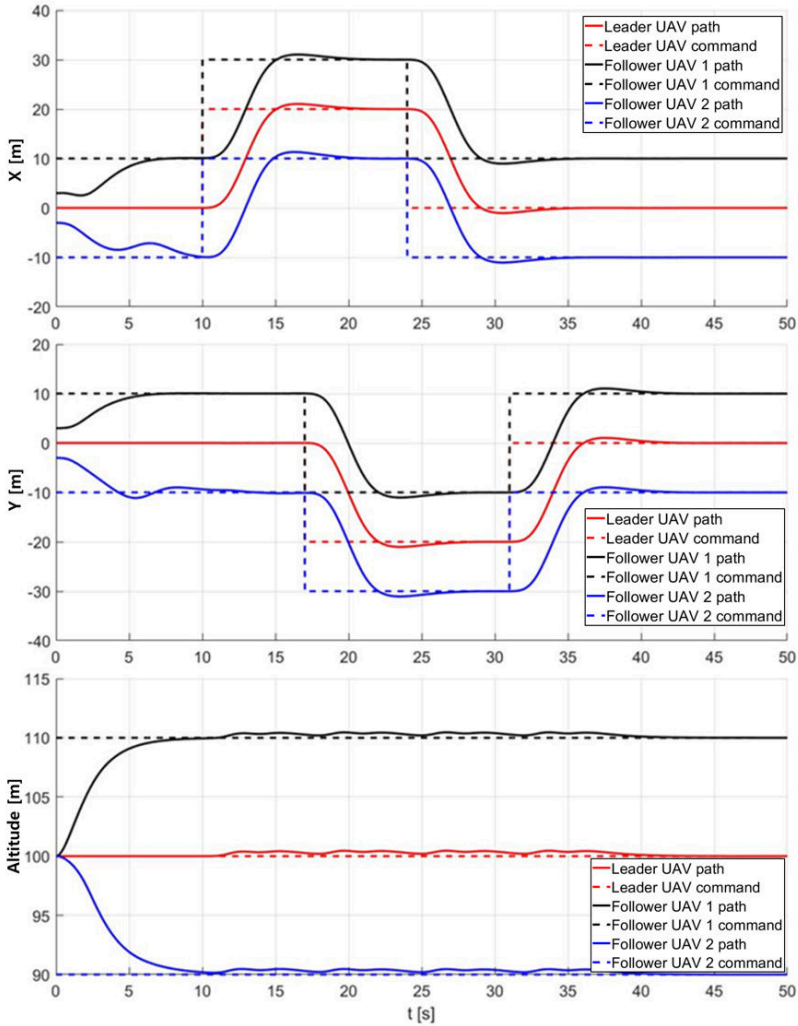


Fig. 8 Position history by the formation flight

2.5.2 Connected flight simulation

In this section, the attitude control system is verified for the connected flight of the DFA system. The attitude control of the connected flight uses a PID controller. This simulation takes hovering flight scenario into account and the interaction due to connection. We consider the DFA system which is composed of three single ducted-fan UAVs. Figure 9 shows the Euler angle when the connected flight hovers for 10 seconds. The dashed line indicates the commands for each Euler angle, and the solid line represents the PID controller. It is seen that some oscillations occur during roll and pitch control due to the influence of interconnection.

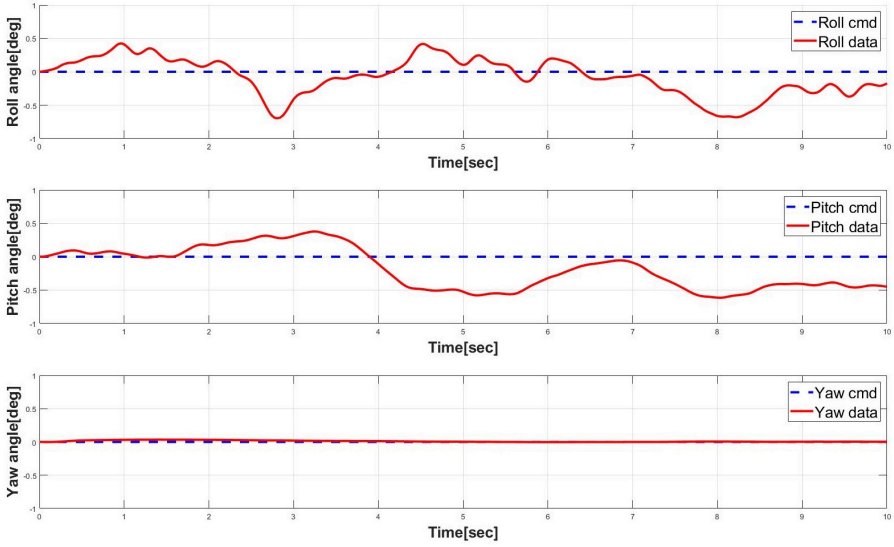
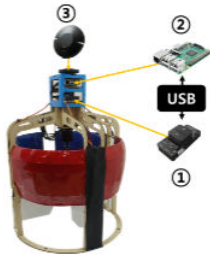


Fig. 9 Responses of Euler angles

2.6 Hardware configuration

The ducted-fan UAV manufactured in-house is equipped with a connected surface and an assembly device on the side to perform connection and separation tasks. Figure 10 exhibits the specifications of the proposed ducted-fan UAV.



Specification	Values
FCC	Pixhawk2.1
Autopilot	Ardupilot
Height	550 mm
Weight	1.63 kg
Endurance	10 minutes
Propeller	14 inch

Fig. 10 Specifications of the ducted-fan UAV

An open-source flight controller board, Pixhawk2.1, controls the ducted-fan UAVs which measures using a 3D gyroscope, 3D accelerometers, and a barometer [27]. This can be connected to an external GPS module and communicate with the mission computer via a protocol called MAVLink [28]. Figure 11 describes the communication architecture of the ducted-fan UAV.

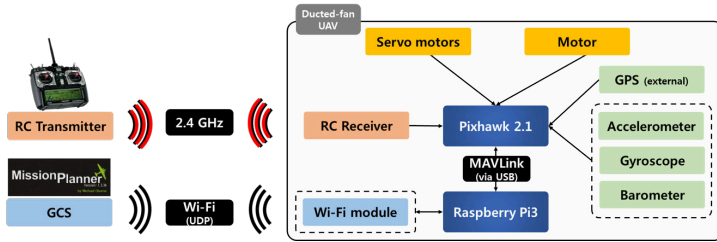


Fig. 11 The ducted-fan UAV communication architecture

2.7 Connecting device

Connecting devices are mounted on the side of the UAV for the combined flight of the ducted-fan UAV. Figure 12 illustrates the design of the connecting devices.

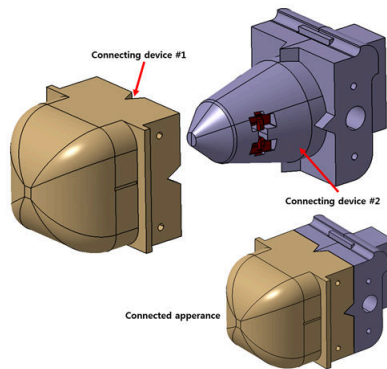


Fig. 12 Design of the connecting device set [22].



Fig. 13 Shape of the connecting device set [22]

The connecting devices #1 and #2 in Figure 12 are closely attached and engaged. Moreover, triangular grooves are added at the device's side, top, and bottom, avoiding gaps depending on the angle of entry of connecting device

#2. Reducing the connecting error when combining UAVs is essential when designing connecting devices. For this, the insertion area was sloped to reduce the connecting error.

Furthermore, the insertion device can smoothly move when disconnected, generating less external force on the UAV. Therefore, the external force generated by the connecting device is minimized during combination and separation. Figure 13 illustrates the shape of the actual connecting device set.

2.8 Communication system for formation flight

In this study, we constructed a DFA communication environment using ROS. The core of the communication environment using ROS is a message communication between nodes, consisting of a Publisher that transmits information, a Subscriber that receives data, and a Master that helps connect nodes. Figure 14 shows the structure of the DFA system built using ROS [29].

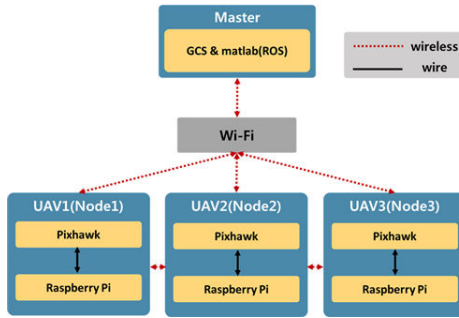


Fig. 14 Architecture of the DFA system

The Master node acquires node information for the Publisher and Subscriber and then passes the data to the Publisher. The DFA system sets the GCS as a Master and each ducted-fan UAV as a node.

3 Flight test

3.1 Single unit flight test

The phased performance verification of the UAV is performed after setting up the ducted-fan UAV in the order of (1) ground test, (2) flight test with tether, and (3) flight test. Figure 15 displays the sequence of the verification tests. The ground test verified the ducted-fan UAV's attitude control performance and controllability. The flight test with a tether confirmed the ducted-fan UAV's altitude and position control performance and proved navigation performance using the waypoint flight.

Figures 16 – 17 demonstrate Euler angle and angular velocity responses of the single unit ducted-fan UAV from the flight tests.



Fig. 15 Verification tests
 URL : <https://www.youtube.com/watch?v=qytc0V32PPg>

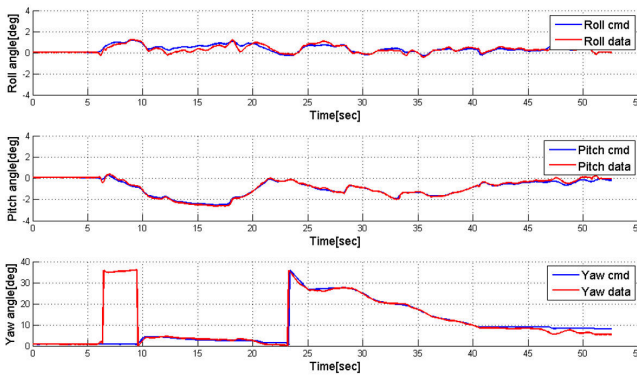


Fig. 16 Result of the flight test (Euler angle)

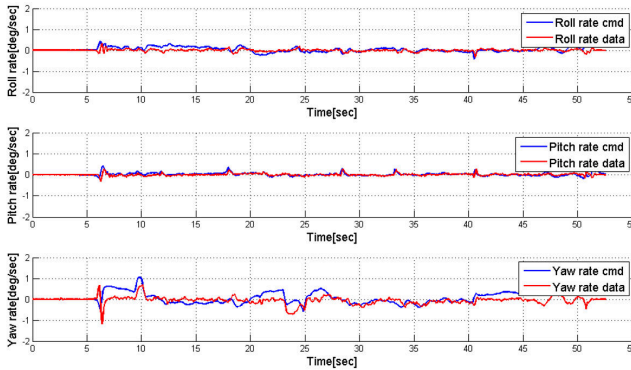


Fig. 17 Result of the flight test (angular velocity)

3.2 Formation flight test

Multiple UAVs were tested for waypoint flight to verify the performance of the formation flight method and the flight communication system of the DFA. Figure 18 shows the formation flight testing of three ducted-fan UAVs.



Fig. 18 UAVs hovering formation flight test
 URL : <https://www.youtube.com/watch?v=8f-PYIOz1QU&t=2s>

Figure 19 exhibits the results of the formation flight test expressed in angular velocity of UAVs. The roll and pitch rate commands follow well, but the yaw rate is hard to track performance because of the characteristics of the ducted fan UAV; the yaw tracking response is slower than other responses.

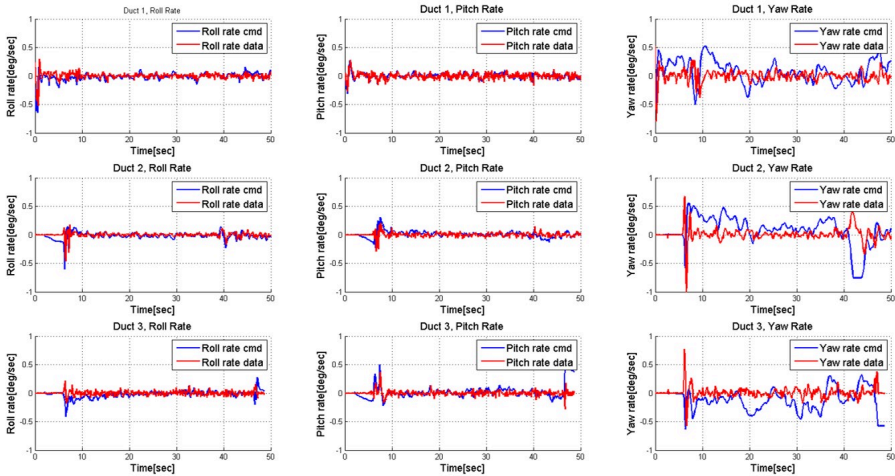


Fig. 19 Result of the formation flight test (angular velocity)

3.3 Connected flight test

Three ducted-fan UAVs are combined into a triangular shape with equally aligned coordinate axes to minimize the change in the center of gravity and maximize the control performance of the connected platform. A tethered flight



Fig. 20 The tethered flight test of connected ducted-fan UAV
<https://www.youtube.com/watch?v=TKajgEEZwiY>

test was carried out after combining the ducted-fan UAVs to test the flight performance during a connected flight. Figure 20 shows the tethered flight tests of the three connected ducted-fan UAVs.

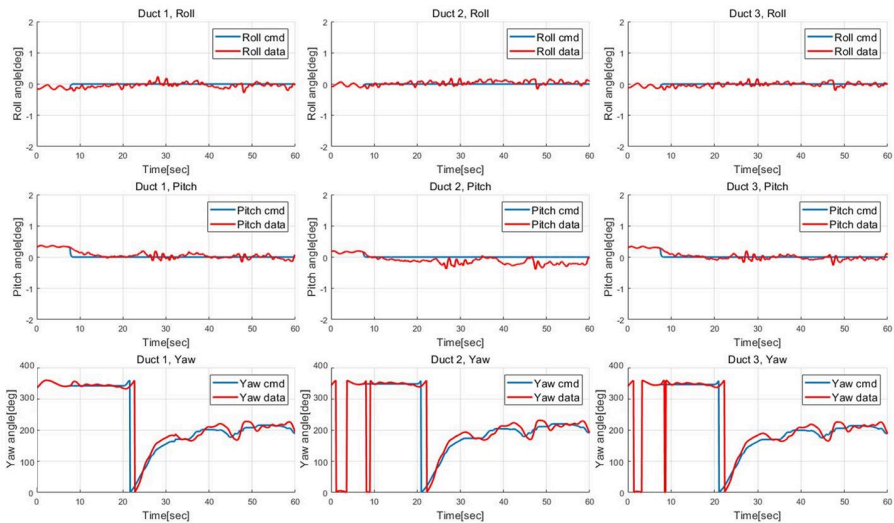


Fig. 21 Connected flight test(Euler angle)

Figure 21 demonstrates the Euler angle when three ducted-fan UAVs were subjected to a connected flight test. The command was applied to the connected ducted-fan UAV in this flight test to perform hovering flight. The resultant graph shows that the roll and pitch axis commands are followed well because

the alignment of the control surfaces of each UAV is matched. However, the attitude command of the yaw axis did not have good tracking performance, unlike the simulation. This result may be caused by clogging the movement of the yaw axis and causing vibration due to the loose coupling of the connecting device.

3.4 Separation flight test

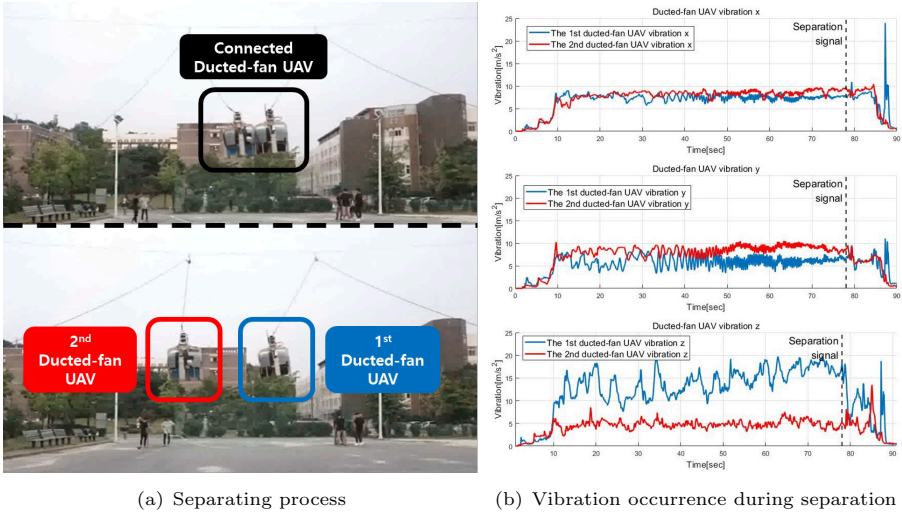
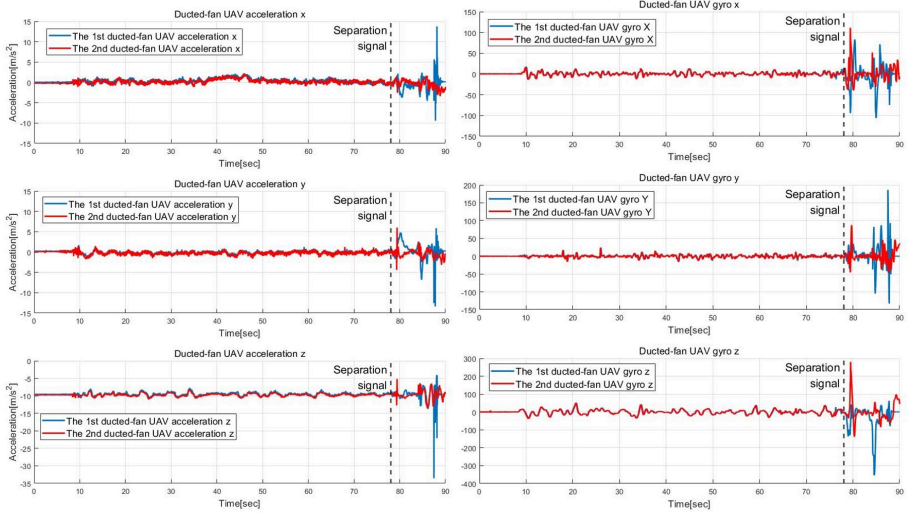


Fig. 22 Separating flight test results
<https://www.youtube.com/watch?v=TKajgEEZwiY>

A hovering flight test was conducted by combining two ducted-fan UAVs to verify the performance of the connecting UAV and check whether it could be separated. The ducted-fan UAVs 1 and 2 were equipped with connecting devices # 1 and # 2, respectively. Figure 22(a) shows separation and hovering flights when an activation signal for separation is applied to the connected UAV. The vibrations of each UAV are shown in Figure 22(b).

The intensity of the vibration in the z-axis is stronger than the vibrations that occurred in other axes, as shown in Figure 22(b). In other words, the vibrations measured in UAV 1 are higher than in UAV 2 during connected-flight conditions. It means that UAV 1 was affected by the vibrations caused when UAV 2 was inserted as device # 2 inside UAV 1. This result could be seen from the decrease in the vibration level measured by UAV 1 after the UAVs were detached. Figure 23 shows the accelerometer and gyroscope measurements during the separation. The ducted-fan UAV 2 reacted when separated, although it shook the ducted-fan UAV 1 for a certain period. The force applied to the device was generated when the connected UAV was separated.



(a) Accelerometer measurements on separation (b) Gyroscope measurements on separation

Fig. 23 IMU sensor measurements on separation

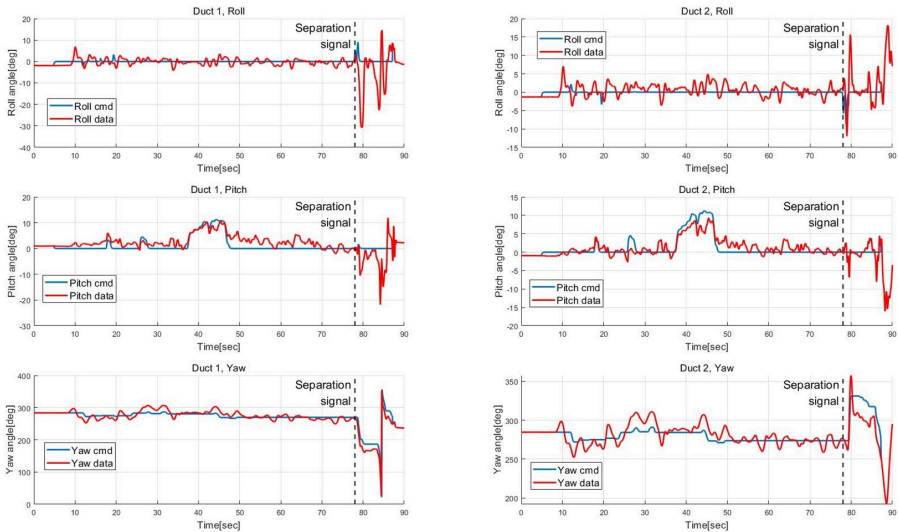


Fig. 24 The Separating mission flight test (Euler angle)

Additionally, Figures 24 and 25 show the Euler angle and angular velocity during the separation of the connected UAVs. When separated, the two UAVs' roll and yaw axes rotate opposite each other, resulting from the reaction force generated when the coupling part of coupling device # 2 (red line in Figure 13) is released.

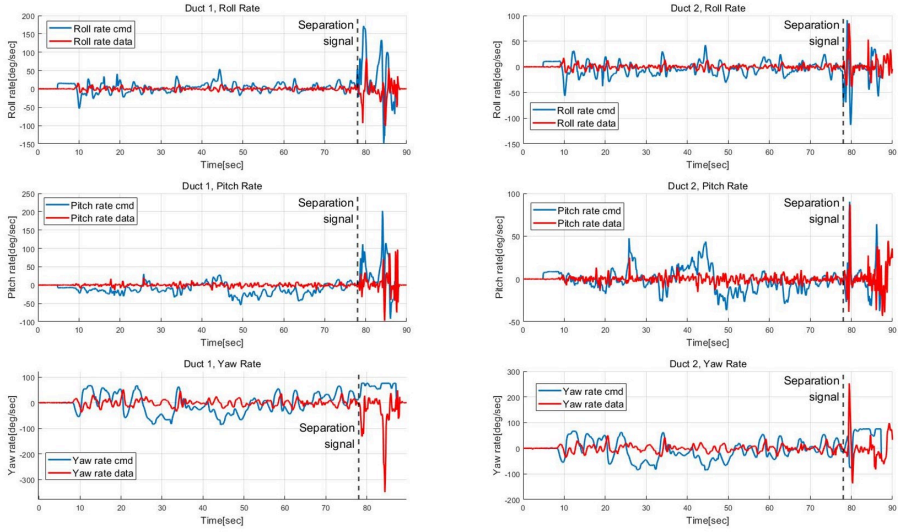


Fig. 25 The Separating mission flight test (angular velocity)

4 Conclusions and Future works

This study proposed a DFA system that changes the configuration of the platform array based on the mission environment. The leader-follower formation flight algorithm was designed and verified numerically and experimentally through actual flights. Moreover, we developed ducted-fan UAVs in-house and an assembly device for DFA missions and constructed the ROS-based communication environment for flight experiments. Subsequently, the performance of the DFA system mission was analyzed through flight tests. It was feasible and applicable to operate the DFA system as an organic flight system that can fly combined and separated.

UAV 1, when operated as a connected array, experienced the vibration more strongly because it received the vibrations generated by other UAVs through the assembly device.

Also, during separation, staggering occurs to the same UAV in the roll and yaw axes due to the reaction force caused by the release of the assembly device.

To cope with the abovementioned problems, we plan to design reconfigurable flight control to adapt to array-shape change and improve the assembly device to absorb or damp the interaction between the UAVs. Furthermore, we will apply robust control against the reaction force, disturbance, and noises generated during connected and separated flight in our future work.

Acknowledgments. This work was supported by research fund of Chungnam National University.

References

- [1] Kim, T., Kim, D., Kim, S., Kim, Y., & Han, S. Improved optical sensor fusion in UAV navigation using feature point threshold filter. *International Journal of Aeronautical and Space Sciences*, 1-12 (2022)
- [2] Cao, Chenkai, Bo Wang, Guoqing Zhao, and Qijun Zhao. "Optimization of Duct Shape for Improving Aerodynamic Performance of Ducted Tail Rotor." *International Journal of Aeronautical and Space Sciences*, 1-17 (2022)
- [3] Oh, B., Jeong, J., Kim, S., & Suk, J. Design of Control System for Organic Flight Array based on Back-stepping Controller. *Journal of the Korean Society for Aeronautical & Space Sciences*, 45(9), 711-723 (2017)
- [4] Zaidi, A., Kazim, M., Weng, R., Wang, D., & Zhang, X. Distributed Observer-Based Leader Following Consensus Tracking Protocol for a Swarm of Drones. *Journal of Intelligent & Robotic Systems*, 102(3), 1-22 (2021)
- [5] Mohammadi, K., Sirouspour, S., & Grivani, A. Control of multiple quad-copters with a cable-suspended payload subject to disturbances.

- IEEE/ASME Transactions on Mechatronics, 25(4), 1709-1718 (2020)
- [6] Deng, S., Wang, S., & Zhang, Z. Aerodynamic performance assessment of a ducted fan UAV for VTOL applications. *Aerospace Science and Technology*, 103, 105895 (2020)
- [7] Cheng, Z., & Pei, H. Hover-to-Cruise Transition Control for High-Speed Level Flight of Ducted Fan UAV. In *2020 International Conference on Unmanned Aircraft Systems (ICUAS)* 1329-1337. IEEE (2020)
- [8] Oung, R., & D'Andrea, R. The distributed flight array. *Mechatronics*, 21(6), 908-917 (2011)
- [9] Muehlebach, M., & D'Andrea, R. The flying platform—a testbed for ducted fan actuation and control design. *Mechatronics*, 42, 52-68 (2017)
- [10] Abedin, J., & Akmeliawati, R. Distributed flight array of autonomous flying vehicles. In *Proceedings of international conference on intelligent unmanned systems* (Vol. 11) (2015)
- [11] Fan, W., Xiang, C., Najjaran, H., Wang, X., & Xu, B. Mixed adaptive control architecture for a novel coaxial-ducted-fan aircraft under time-varying uncertainties. *Aerospace Science and Technology*, 76, 141-154 (2018)
- [12] Fan, W., Xu, B., Zhang, Y., Tang, S., & Xiang, C. Adaptive fault-tolerant control of a novel ducted-fan aerial robot against partial actuator failure. *Aerospace Science and Technology*, 107371 (2022)
- [13] Jeong, J., Kim, S., & Suk, J. Control performance analysis on variable configuration of ducted-fan flight array. *International Journal of Aeronautical and Space Sciences*, 21(2), 524-537 (2020)
- [14] Jeong, Junho. "Dynamics and control of ducted-fan flight array system." Ph. D. thesis, (2017)
- [15] Kim, T., Jang, Y., Kim, M., Jeong, J., Suk, J., & Kim, S. Development and flight test of an electric powered small ducted-fan UAV. In *Proceedings of the Korean Society for Aeronautical & Space Sciences 2017 Spring Conference, Gangwon, Republic of Korea* 210-211 (2017)
- [16] Drela, M., & Youngren, H. Axisymmetric analysis and design of ducted rotors. *DFDC Software Manual* (2005)
- [17] Pereira, J. L. Hover and wind-tunnel testing of shrouded rotors for improved micro air vehicle design. University of Maryland, College Park (2008)

- [18] Andrikopoulos, G., & Nikolakopoulos, G. Vortex actuation via electric ducted fans: an experimental study. *Journal of Intelligent & Robotic Systems*, 95(3), 955-973 (2019)
- [19] Jeong, J., Kim, S., & Suk, J. Control system design for a ducted-fan unmanned aerial vehicle using linear quadratic tracker. *International Journal of Aerospace Engineering*, (2015)
- [20] Guerrero, I., Londenberg, W. K., Gelhausen, P., & Myklebust, A. A powered lift aerodynamic analysis for the design of ducted fan uavs. In 2nd AIAA" Unmanned Unlimited" Conf. and Workshop & Exhibit (p. 6567) (2003, September)
- [21] Wang, Z., Liu, Z., Fan, N., & Guo, M. Flight dynamics modeling of a small ducted fan aerial vehicle based on parameter identification. *Chinese Journal of Aeronautics*, 26(6), 1439-1448 (2013)
- [22] Jeaong, H., Kim, T., Kim, S., Yang, S., Jeong, J, Kim, S., & Suk, J. Development and Validation of Mechanical Device for Assembly or Separation of Multiple UAVs", *Proceedings of the Korean Society for Aeronautical & Space Sciences 2017 Fall Conference*, 535-536, (2017)
- [23] Jeong, J., Kim, S., & Suk, J. Adaptive sliding mode controller design for reconfiguration of organic flight array, *In 30th Congress of the International Council of the Aeronautical Sciences*, (2016)
- [24] Wang, N., Dai, J., & Ying, J. UAV formation obstacle avoidance control algorithm based on improved artificial potential field and consensus. *International Journal of Aeronautical and Space Sciences*, 22(6), 1413-1427 (2021)
- [25] Park, S. Rendezvous guidance on circular path for fixed-wing UAV. *International Journal of Aeronautical and Space Sciences*, 22(1), 129-139 (2021).
- [26] Turpin, M., Michael, N., & Kumar, V. Trajectory design and control for aggressive formation flight with quadrotors. *Autonomous Robots*, 33(1), 143-156 (2012)
- [27] Meier, L., Tanskanen, P., Fraundorfer, F., & Pollefeys, M. Pixhawk: A system for autonomous flight using onboard computer vision. *In 2011 IEEE International Conference on Robotics and Automation 2992-2997* IEEE (2011)
- [28] Meier, L., Camacho, J., Godbolt, B., Goppert, J., Heng, L., & Lizarraga, M. Mavlink: Micro air vehicle communication protocol. (2013)

- [29] Kim, T., Kim, S., & Suk, J. Formation Flight Simulation and Flight Test of Multiple Ducted-fan UAV, *Journal of Institute of Control, Robotics and Systems*, 25(5), 398-406 (2019)

2023-02-24

Design and flight testing of the ducted-fan UAV flight array system

Kim, Taegyun

Springer

Kim T, Jeaong H, Kim S, et al., (2023) Design and flight testing of the ducted-fan UAV flight array system. *Journal of Intelligent and Robotic Systems*, Volume 107, February 2023, Article number 32

<https://doi.org/10.1007/s10846-023-01821-6>

Downloaded from Cranfield Library Services E-Repository